Preliminary interpretation of high-resolution aeromagnetic data collected near Taos, New Mexico

V. J. S. Grauch, P. W. Bauer, and K. I. Kelson
2004, pp. 244-256. https://doi.org/10.56577/FFC-55.244

in:

Geology of the Taos Region, Brister, Brian; Bauer, Paul W.; Read, Adam S.; Lueth, Virgil W.; [eds.], New Mexico Geological Society 55 th Annual Fall Field Conference Guidebook, 440 p. https://doi.org/10.56577/FFC-55

This page is intentionally left blank to maintain order of facing pages.

PRELIMINARY INTERPRETATION OF HIGH-RESOLUTION AEROMAGNETIC DATA COLLECTED NEAR TAOS, NEW MEXICO

V. J. S. GRAUCH[1], PAUL W. BAUER[2] AND KEITH I. KELSON[3]
[1]U. S. Geological Survey, MS 964, Federal Center, Denver, CO 80225;
[2]New Mexico Bureau of Geology and Mineral Resources, Socorro, NM 87801;
[3]William Lettis & Associates, Inc., 1777 Botelho Dr, Suite 262, Walnut Creek, CA 94596

ABSTRACT.—High-resolution aeromagnetic data were recently collected in an area surrounding the Town of Taos to improve the regional geologic understanding of the subsurface. Qualitative and quantitative analyses of the data were integrated to obtain a preliminary interpretation. The primary sources of aeromagnetic anomalies are interpreted as Servilleta Basalt with dominantly reversed-polarity remanent magnetization, weakly to moderately magnetic Precambrian crystalline basement, and magnetic Tertiary intrusions. In the western part of the survey area, we interpret an area of shallow Servilleta Basalt cut by north-striking faults, which are related to the Los Cordovas faults. The area of shallow basalt is faulted down to the east on the eastern side, and is truncated by northeast-striking faults near the Rio Pueblo de Taos on the southern side. A basement structural bench under the Town of Taos, which appears to be bounded by some of the northeast-striking faults, likely continues into a structurally complex area underlying the Buffalo Pasture area, but the configuration is unclear. In the northeastern part of the survey area, we interpret rift-related and pre-rift faults that strike north and northwest, respectively. The north-striking faults align with the Rio Lucero, supporting the premise that the drainage is tectonically controlled. Faults of both orientations appear to bound basement structural benches that step down to the south and west. In the southern and east-central parts of the area, aeromagnetically inferred faults parallel major variations in orientation of the Embudo, Sangre de Cristo and Picuris-Pecos fault systems. The parallel faults occur within a 2- to 7-km-wide zone from the range front into the basin. We interpret high-amplitude aeromagnetic anomalies along the northern and northeastern survey perimeters to represent Tertiary plutons, which are partially exposed and intrude Precambrian rocks in the north. Similar anomalies just north of Rio Pueblo de Taos are likely caused by a related Tertiary pluton that is buried beneath Paleozoic sedimentary rocks.

INTRODUCTION

The Town of Taos, Taos Pueblo, and surrounding communities are located in the structurally and stratigraphically complex Taos embayment (Bauer and Kelson, 2004), which forms the southeasternmost portion of the San Luis Basin segment of the northern Rio Grande rift (Fig. 1). Rapidly increasing population, continued drought, and disputes over water rights have driven water resource managers to explore for deeper aquifers than have been traditionally utilized for groundwater (Drakos and Lazarus, 1998). However, the combination of complex geology, extensive alluvial cover, and inadequate subsurface information has prevented a complete understanding of the regional geologic and hydrogeologic framework of the area (Bauer et al., 1999a).

To help improve understanding of the regional geology, a high-resolution, helicopter aeromagnetic survey was conducted over the Taos area in October 2003 (Bankey et al., 2004). In the central Rio Grande rift to the south, analyses of high-resolution aeromagnetic surveys were successful in locating concealed faults, defining the extent of buried igneous rocks and lava flows, and estimating depths to basement structural blocks (Grauch, 1999; Grauch et al., 2002; Grauch and Bankey, 2003). Locating these features improved the understanding of subsurface controls on ground water flow and/or water quality and helped provide estimates on the overall thickness of the basin-fill aquifer (Grauch and Bankey, 2003; Phillips and Grauch, 2004).

This paper presents preliminary geologic interpretations of the high-resolution aeromagnetic data flown over the Taos area (Fig. 1; Plate 5). The interpretations integrate qualitative and quantitative analyses to define the overall configuration of basement blocks, basalt flows, and faults in the subsurface and provide rough estimates of the depths to these features. More detailed modeling and analysis in conjunction with well data and other

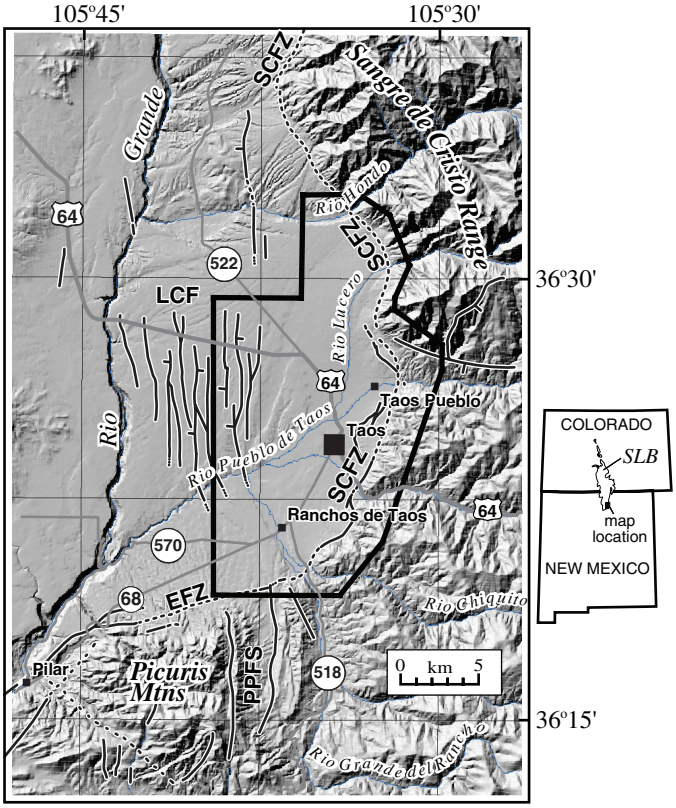

FIGURE 1. Location of the high-resolution aeromagnetic survey area (bold outline) with respect to topography (shaded-relief), geography, and mapped faults (hachure on downthrown side; dashed where inferred). Faults are from Machette and Personius (1984) and the state geologic map (New Mexico Bureau of Geology and Mineral Resources, 2003). EFZ=Embudo fault zone; LCF=Los Cordovas faults; PPFS=Picuris-Pecos fault system; SCFZ=Sangre de Cristo fault zone. Index map shows location of map area within the San Luis Basin (SLB).

geophysical data are required to fully utilize the information contained in the aeromagnetic data.

GEOLOGIC SETTING

The Taos area is located in southeastern San Luis Basin, a large extensional basin of the northern Rio Grande rift that spans northern New Mexico and southern Colorado (Fig. 1). At the latitude of Taos, the basin contains a thick section of Tertiary clastic sedimentary rocks and a variety of Oligocene to Pliocene volcanic rocks. West of the Rio Grande, most of the southern basin is capped by nearly flat-lying basalt flows of the Pliocene Servilleta Formation, which are part of the Taos Plateau volcanic field (Plate 2). Individual flows exposed in the Rio Grande gorge, which are up to 12 m thick, are grouped into packages of from one to ten flows, separated by sedimentary intervals of variable thickness (Leininger, 1982; Dungan et al., 1984). Packages can be up to 150 m thick (Dungan et al., 1984). East of the Rio Grande, Servilleta basalt flows are irregularly exposed under extensive Pleistocene and Holocene alluvial deposits, which cover most of the Taos area (Plate 6).

The Taos area is flanked by the Sangre de Cristo Range to the east and the Picuris Mountains block on the south (Fig. 1). Exposures in the mountains northeast of Taos consist of Precambrian plutonic and metamorphic rocks intruded by Tertiary granitic rocks (Plate 6; Lipman and Reed, 1989). Northeast of Taos Pueblo, Pennsylvanian sedimentary strata are downdropped against Precambrian granitic rocks along a west-northwest-striking, high-angle fault (Plate 6; Fig. 1). South of the fault, an unknown thickness of Paleozoic sedimentary rocks overlies the Precambrian basement (Bauer and Kelson, 2001). The sedimentary rocks were deposited in the Late Paleozoic, north-trending Taos trough, which may contain as much as 1800 m of sedimentary section east of Taos (Baltz and Myers, 1999). The Picuris Mountains contain a variety of Precambrian rocks, including felsic and mafic metasedimentary and metavolcanic rocks of the Hondo and Vadito Groups and a series of granitic plutons (Bauer, 1993).

The curved mountain front around the Taos area corresponds to a structural embayment in the San Luis Basin (Taos embayment) formed by the Embudo and Sangre de Cristo fault zones (EFZ and SCFZ on Fig. 1; Bauer et al., 1999b; Bauer and Kelson, 2001). The Embudo fault zone is a left-oblique, north-down rift transfer zone that separates the east-tilted San Luis Basin from the west-tilted Española Basin to the south (Faulds and Varga, 1998; Bauer and Kelson, 2004; Kelson et al., 2004). The Sangre de Cristo fault zone is a steeply west-dipping, normal fault system that bounds the west flank of the Sangre de Cristo Mountains for 160 km along the eastern margin of the San Luis Basin. The transition between the Embudo and Sangre de Cristo fault zones occurs at the intersection with a third major fault system, the Picuris-Pecos fault system (PPFS on Fig. 1). This system is composed of multiple high-angle, north-striking parallel faults that separate the Picuris Mountains block from the main block of the Sangre de Cristo Range. The Picuris-Pecos fault system, which has been active repeatedly since Precambrian time, can be followed at least 84 km to the south (Bauer and Ralser, 1995). A 5- to 8-km-wide zone of Pleistocene-age, intra-rift faults, the Los Cordovas faults (LCF on Fig. 1; Lambert, 1966; Machette and Personius, 1984), generally aligns with the northern extension of the Picuris-Pecos fault system. The faults are north-striking, generally west-down, and juxtapose piedmont-slope alluvium against older Servilleta Basalt (Kelson and Bauer, 2003).

Regional gravity data indicate that the southern San Luis Basin contains a deep (>3 km), north-elongate graben between Taos and the Rio Grande (Keller et al., 1984; Grauch and Keller, 2004), resulting in a rift basin (Taos graben) that is less than half the width of the topographic valley. The western graben border approximately follows the Rio Grande (Cordell and Keller, 1984; Grauch and Keller, 2004). The eastern graben border coincides with the Sangre de Cristo fault zone north of the Taos embayment, but is buried under extensive Pleistocene and Holocene alluvial deposits within the embayment. Bauer and Kelson (2004) theorized that the eastern graben border within the embayment is a transitional zone formed by the northward extension of the buried Picuris-Pecos fault system and evidenced by the Los Cordovas faults. East of this zone they suggested that a shallow structural bench underlies Taos and represents an intermediate level in the stepped, eastern rift margin.

AEROMAGNETIC DATA

Aeromagnetic data, which are collected during airborne geophysical surveys, measure subtle variations in the Earth's magnetic field. The surveys are designed to focus on those variations that are caused by differences in the magnetic properties of underlying rocks. The aeromagnetic survey for the Taos area (Fig. 1) employed a helicopter flying along traverse lines oriented east-west, spaced 200 m apart, and flown a nominal 150 m (500 ft) above ground (Bankey et al., 2004). Orthogonal lines were flown north-south at a 1000-m spacing. The survey was flown closer to the ground and with narrower line spacing than conventional aeromagnetic surveys to obtain high-resolution map images and to better detect weakly magnetic rocks. This high resolution facilitates interpretation of aeromagnetic data by allowing easier discrimination between different patterns and shapes that relate to their corresponding geologic origin. Use of a helicopter was required to maintain low clearance along the range front. The east-west orientation of traverse lines was chosen because this direction is oblique to the predominant northerly to northeasterly geologic strike of the area (Plate 6).

After standard processing, the data were interpolated onto a grid at 50-m intervals. The gridded data were then downward continued to simulate data acquired at 100 m above ground and reduced to the pole (Bankey et al., 2004), following common practice (Blakely, 1995). Downward continuation significantly enhances the details in aeromagnetic maps. The reduction-to-pole (RTP) transformation corrects for the offset between the locations of anomalies (closed highs or lows on a contour map) and their sources that is a consequence of the vector nature of the Earth's magnetic field. To apply the reduced-to-pole transformation correctly, one must assume that the total magnetizations of most rocks in the study area align parallel or anti-parallel to the Earth's

main field (declination=10°, inclination=64° for the study area). The collinearity assumption probably works well for this area, because the rocks most likely to have large remanent magnetizations formed during Tertiary time, when the direction of the Earth's field was similar to the present-day orientation (Butler, 1992). The downward continued, reduced-to-pole aeromagnetic data are shown as a color shaded-relief image in Plate 5a.

Both geologic and non-geologic sources are represented by anomalies on the aeromagnetic map (Plate 5a). The non-geologic, anthropogenic sources are characterized by spatially limited anomalies with well-defined edges, such as the pock-like anomalies within the limits of the Town of Taos. From inspection of 1:24,000 base maps, most of the sources can be identified as structures constructed with a substantial amount of steel, such as large commercial or institutional buildings, sizeable stock tanks, and electrical substations. The anomalies are easy to recognize during qualitative interpretation, but hard to separate from anomalies of interest before quantitative analysis, especially where they are clustered (Muszala et al., 2001). A northwest-trending, elongate anomaly south of US-64 and west of the intersection with NM-522 (LF on Plate 5a) is produced by a large landfill.

ROCK MAGNETIC PROPERTIES

Aeromagnetic maps represent magnetic-field variations caused by differences in the *total magnetization* of underlying sources. Total magnetization is the vector sum of induced and remanent components. The induced component of a rock is the product between the Earth's present-day magnetic field vector and the magnetic susceptibility. Magnetic susceptibility is a scalar measure of the quantity and type of magnetic minerals (commonly titanomagnetites) in the rock. The remanent component (also a vector) is based on the permanent alignment of magnetic domains within magnetic minerals and is measured using paleomagnetic methods (Butler, 1992).

Igneous and crystalline metamorphic rocks commonly have high total magnetizations compared to other rock types, whereas sedimentary rocks and poorly consolidated sediments have much lower magnetizations (Reynolds et al., 1990; Hudson et al., 1999). Total magnetizations of volcanic rocks are normally dominated by the remanent component, whereas those for all other rock types are dominated by the induced component, with the exception of some mafic metamorphic rocks (Reynolds et al., 1990; Clark, 1997). Aeromagnetic anomalies over volcanic rocks commonly produce high-amplitude positive or negative anomalies. Where a correspondence between volcanic edifices and anomaly shape can be demonstrated, positive and negative anomalies indicate normal and reversed-polarity remanent polarities of the rocks, respectively. A correlation between age, remanent magnetic polarity, and negative versus positive aeromagnetic anomalies has been demonstrated for basaltic rocks just west and northwest of the study area in the Taos Plateau (Grauch and Keller, 2004) and in the Cerros del Rio volcanic field to the south near Santa Fe (Hudson et al., 2004).

Limited information on magnetic properties exists for rocks of the Taos area. However, based on rock type, potential sources of anomalies are Tertiary igneous and perhaps volcaniclastic rocks, and Precambrian crystalline rocks. Remanent magnetizations of numerous samples of Servilleta Basalt gave values that are relatively small (1 A/m) in comparison to neighboring intermediate-composition volcanic rocks (≥10 A/m) in an extensive paleomagnetic study of the Taos Plateau volcanic field west of the survey area (Brown et al., 1993). In the same study, paleomagnetic samples from several stratigraphic sections of Servilleta Basalt within the Rio Grande gorge consistently yielded normal polarities for the uppermost basalts and dominantly reversed polarities for underlying flows. However, surface samples from a wider area showed both normal and reversed polarities, which largely precludes establishing a simple correlation between polarity and volcanic stratigraphy. Furthermore, remanent polarities cannot be predicted based on expected age of basalt, because the ~2.5 Ma span of radiometric age dates from basalt flows in the gorge (Appelt, 1998) includes multiple magnetic polarity events (Grauch and Keller, 2004). The negative aeromagnetic anomalies observed over exposures of Servilleta Basalt (Plate 5a) are the best evidence that the upper section of Servilleta Basalt in the Taos area is dominated by flows with reversed-polarity remanent magnetization. Clearly more work is required to understand the stratigraphic correlation between these flows and those located elsewhere.

The magnetic properties of Precambrian basement rocks in the Taos area are not known from surface samples, but are demonstrably highly variable by inspection of regional aeromagnetic data for the surrounding mountains. From the wide range of anomaly amplitudes, the regional data suggest that Precambrian rocks are weakly magnetic in the Picuris Mountains where the rocks are primarily metasedimentary, moderately magnetic in the Sangre de Cristo Range just north of the study area where the rocks are generally plutonic, and strongly magnetic south of the Picuris Mountains, where rock types are mixed and the magnetic source is unclear (Grauch and Keller, 2004).

APPROACH TO INTERPRETATION

Aeromagnetic interpretation commonly involves qualitative and quantitative analyses that are integrated to arrive at a geologic interpretation of the subsurface. Qualitative analysis involves examination of anomaly patterns to determine the character of particular geologic units in order to infer their presence in the subsurface. Quantitative analysis involves application of a set of analytical methods to the data to constrain the shape of and depth to magnetic "sources". Integration of these analyses into a geologic interpretation is usually an iterative process and highly dependent on the quality and resolution of the data, the variability and spatial distribution of magnetic properties, geologic complexity, interference from unrelated magnetic sources such as urban structures, and the amount of independent information available to help constrain ambiguities.

The following sections describe the qualitative and quantitative analyses applied to the Taos high-resolution aeromagnetic data. To illustrate geophysical concepts, interpretive conclusions, and application of analytical techniques during the discussion, we

constructed a hypothetical model to simplistically represent the configuration of the two main magnetic sources anticipated in the survey area (Fig. 2). The model includes a series of thin magnetic layers that are offset from each other to represent faulted sections of Servilleta Basalt (shaded bodies A-E) and a deeper, thicker, stepped body to represent faulted crystalline Precambrian basement (patterned body). The model bodies were given total magnetizations of 0.52 A/m for the basalt, assumed to be dominated by reversed-polarity remanence, and 0.26 A/m for the crystalline basement, assumed to be dominated by the induced component (magnetic susceptibility of 0.0063 SI). Although these values are arbitrary, they were adjusted to produce anomalies that are similar in sign and amplitude to typical observed anomalies (Plate 5a). Paleozoic and Tertiary sedimentary sections known to overlie the Precambrian rocks (Bauer and Kelson, 2004) are not modeled because their magnetizations are considered negligible in comparison to the main magnetic sources. Magnetic sources related to Tertiary volcaniclastic rocks (Picuris Formation) may occur at depth. Their depth and extent are poorly known, so they are not considered in the model for simplicity.

QUANTITATIVE ANALYSIS

The quantitative techniques applied to the Taos high-resolution aeromagnetic data rely on analysis of anomaly slopes to locate edges of magnetic sources and to estimate depths to the tops of these edges. The analyses use the magnitude of horizontal gradient to measure anomaly slope, and are based on the mathematical behavior of magnetic fields over idealized magnetic source edges and the general principle that anomalies due to shallow sources have steeper slopes than those that are deep.

Location of Magnetic Source Edges

The edges of magnetic sources represent abrupt lateral rock-property contrasts that occur at faults or steeply dipping contacts.

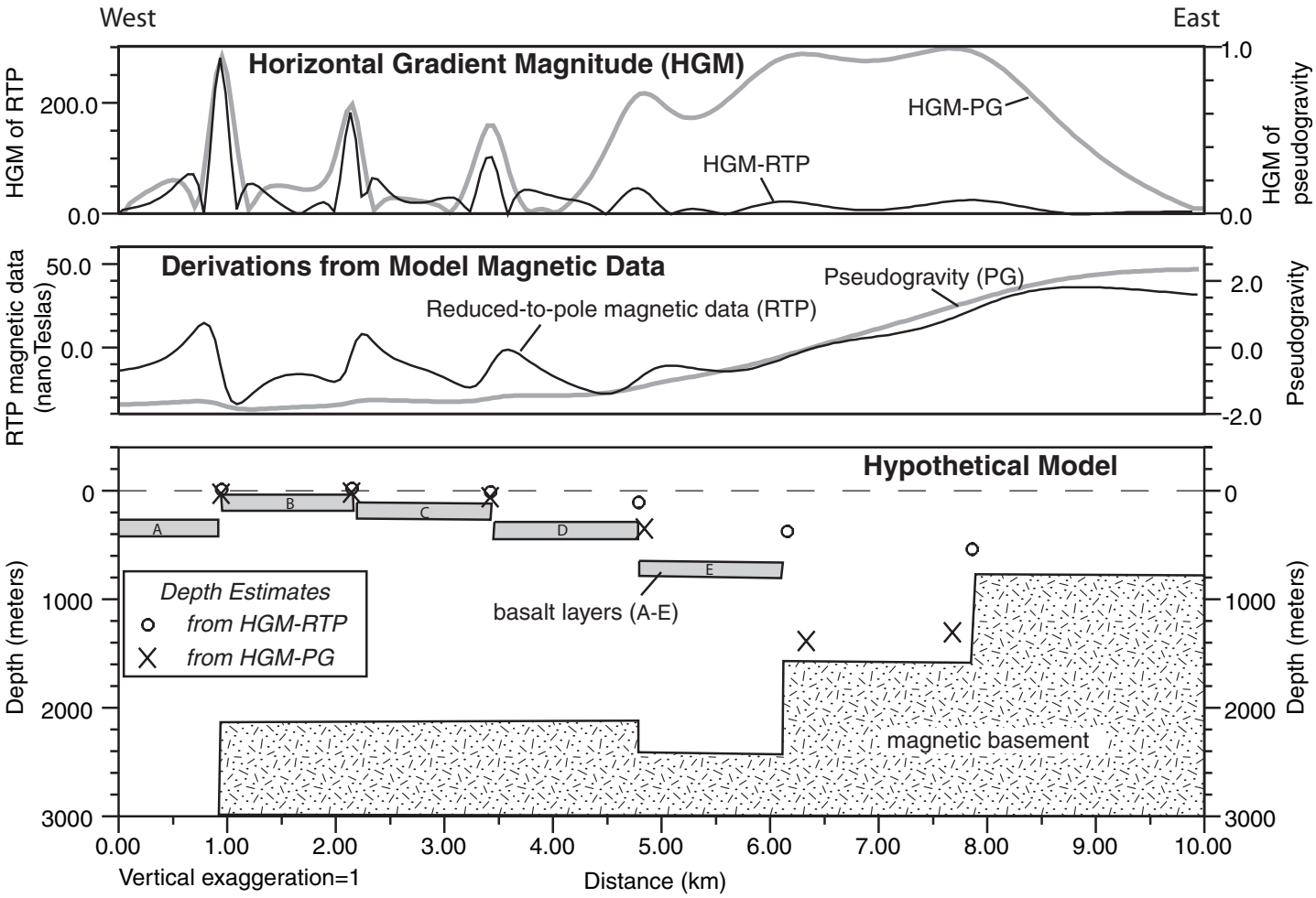

FIGURE 2. Hypothetical model constructed to illustrate concepts of anomaly interpretation and depth estimation. No attempt is made to fit observed data. Idealized bodies were constructed for magnetic (crystalline) basement and basalt flows, which were given total magnetizations of 0.26 A/m (assumed to be dominantly induced) and -0.52 A/m (assumed to be dominantly reversed-polarity), respectively. Calculated reduced-to-pole (RTP) magnetic and pseudogravity (PG) curves and the respective horizontal-gradient magnitudes (HGM) of these curves are shown to accompany discussion in text. Depth solutions (depth estimates) derived from HGM-RTP (circle) and HGM-PG (X) using algorithm of Phillips (1997; Program PDEPTH) are shown only for the most prominent peaks.

The horizontal-gradient method is commonly used to detect magnetic source edges semi-automatically, using the horizontal gradient magnitude of pseudogravity data (Cordell and Grauch, 1985; Blakely and Simpson, 1986) or reduced-to-pole magnetic data (Phillips, 2000; Grauch et al., 2001). Pseudogravity data, also called the magnetic potential, is a vertical integral of the reduced-to-pole magnetic data (Baranov, 1957; Blakely, 1995). The pseudogravity data (which have nothing to do with the observed gravity field) are derived from the original aeromagnetic data, but enhance the broad features at the expense of the details, as demonstrated by comparing the pseudogravity and reduced-to-pole curves computed for the hypothetical model (Fig. 2).

The slopes of pseudogravity or reduced-to-pole curves over magnetic sources are steepest over near-vertical edges. The steepest slopes are found from the maximum of the magnitude of the horizontal gradient, analogous to computing a derivative to find the inflection point of a curve. Horizontal gradient magnitude (HGM) curves that peak over magnetic source edges are demonstrated by the two upper curves derived from reduced-to-pole and pseudogravity data of the hypothetical model (HGM-RTP and HGM-PG on Fig. 2). The HGM curves have sharp, high-amplitude peaks over the shallowest edges (basalt layers B and C on Fig. 2), reflecting the sensitivity of magnetic data to shallow sources. The amplitudes decrease and peaks widen over the deeper sources (basalt layer E and crystalline basement on Fig. 2). Over the edges of the shallow sheet-like sources (e.g., layer B on Fig. 2), both reduced-to-pole and pseudogravity HGM curves show a prominent peak flanked by one to two peaks with lesser magnitudes. This type of HGM signature reflects the finite depth extent of the magnetic source edge, but the flanking peaks can be easily misinterpreted as multiple edges in practice. The problem is generally less for the HGM of pseudogravity (compare the HGM curves over the east edge of layer B) and for the HGM of both curves for the deeper sources (e.g., basalt layer D and the easternmost step in the magnetic basement on Fig. 2).

To minimize potential misinterpretation of multiple peaks, we relied on the HGM of the pseudogravity to trace peaks representing magnetic source edges (Fig. 3). The results are similar to those obtained from automated depth-estimation methods (Plate 5b), except that only the strongest and most continuous gradients are represented. The interpreted edges are inferred to represent primarily faults because of their linearity. This interpretation is supported by HGM maxima that closely parallel or coincide with mapped fault strands (Fig. 3). Five different structural domains were recognized within the survey area by differences in inferred fault patterns, such as general orientation and spacing (Fig. 3). These domains help focus discussion of the geologic interpretation in later sections.

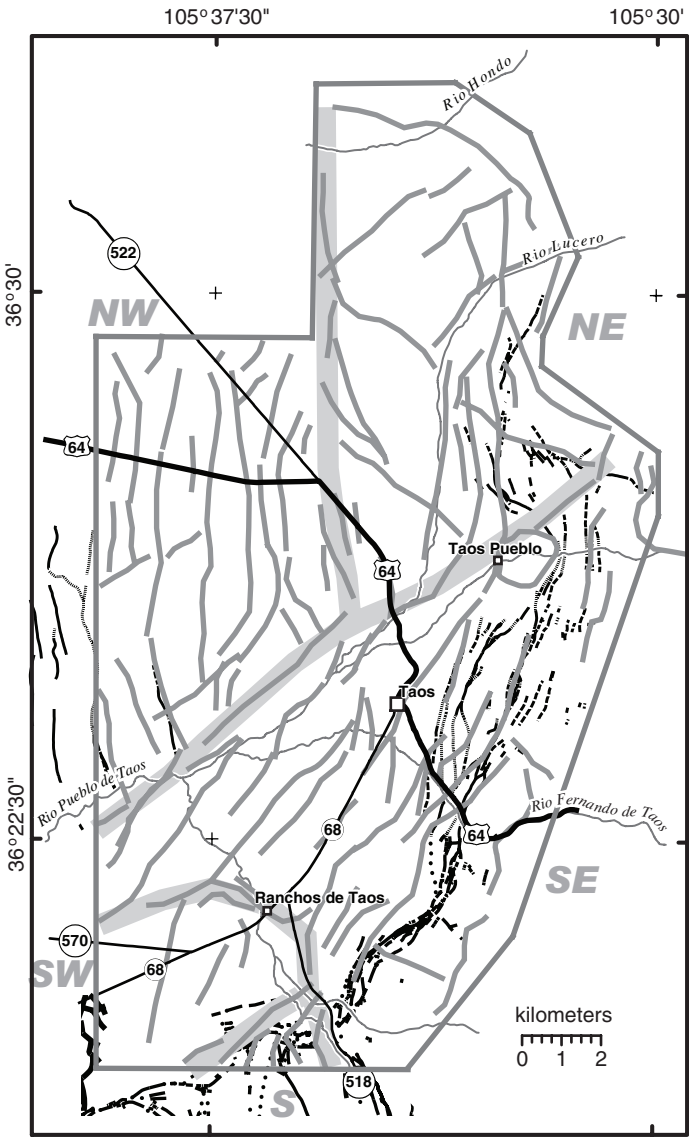

FIGURE 3. Locations of interpreted magnetic source edges, derived by tracing ridge crests from the horizontal-gradient magnitude (HGM) of pseudogravity (transformed aeromagnetic data). Most edges are inferred as faults. Variations in patterns are divided by structural domain (broad gray lines), including the northwestern (NW), southeastern (SE), southwestern (SW), southern (S), and southeastern (SE) domains discussed in text. Mapped faults from Bauer et al. (1999b), Bauer and Kelson (2001), and Kelson and Bauer (2003).

Depth Estimation

The HGM curves can be used to estimate depths to the tops of magnetic edges using the principle that shallow sources generate anomalies with steeper gradients than those produced by similar, deep sources. In the hypothetical model, this principle is demonstrated by the greater widths of HGM curves that define the peaks over the edges of the deep versus shallow basalt layers (Fig. 2). Algorithms that solve for depth from the HGM of reduced-to-pole data or pseudogravity give minimum and maximum estimates of depth to the tops of magnetic source edges, respectively (Phillips, 2000). These estimates together give a range of values within which the actual depth is likely to fall.

The advantages of the HGM depth-estimation technique over the many other existing techniques (see Blakely, 1995, for example) are its low sensitivity to noise (Phillips, 2000) and its applicability to maps rather than individual profiles (program HDEP in Phillips, 1997). The main disadvantages are that depth estimates give only ranges of values that are sometimes too large to

be useful and the resolution of near-surface sources is poor when used for map data. Like all depth estimation methods, the results are subject to problems related to interference from neighboring or underlying sources, complexities in the geometry of source edges, variations in thickness of sources, and high variability of magnetic properties.

The types of results anticipated for the Taos data are demonstrated by the hypothetical model (Fig. 2). Depths were computed (program PDEPTH of Phillips, 1997) using HGM from both reduced-to-pole (circle) and pseudogravity (x) calculated from the model (Fig. 2). For simplicity, depth solutions associated with only the most prominent of multiple peaks in the HGM curves were retained. Depth solutions from the HGM of both reduced-to-pole and pseudogravity are similar over the shallow basalt layers (B-C), with both giving fairly good results. The separation between the two types of solutions is greater over the deeper magnetic source edges (the easternmost fault in the magnetic basement on Fig. 2), where the depth solutions bracket the actual depth to the top of the magnetic edge and thereby demonstrate their use as minimum and maximum estimates. Note the lack of deep solutions on the west side of the model, where the strong anomalies associated with the shallow sources mask the weak anomalies produced from the deep parts of the modeled magnetic basement.

Although the depth estimates for the hypothetical model are illustrative, estimates computed from observed aeromagnetic data are subject to ambiguities that are often difficult to resolve. In the Taos area, accurate depth estimates to the top of Servilleta Basalt depend on several assumptions: (1) the top basalt layer is representative of the flow package as whole, (2) the flow package has significant thickness and large enough magnetization to produce aeromagnetic anomalies at its present depth level, (3) individual flows were originally emplaced with relatively constant thickness and homogeneous magnetization, and (4) contributions to the aeromagnetic anomalies from underlying rocks are insignificant. From the large variations in the thickness of basalt intervals and of flow packages as a whole observed in wells (Table 1), the first two assumptions are problematic. Other assumptions may be generally valid in regions of the survey area, but information is insufficient. Thus, the depth estimates from the quantitative analysis should not be taken literally. Careful examination of depth estimates in relation to well data in local areas may be a good direction for future work.

Depth solutions were determined for the Taos data from the gridded HGM of both reduced-to-pole data and pseudogravity (Plate 5b) (Phillips, 1997; program HDEP). In this procedure, depth solutions are only computed where linear trends can be determined within a moving window. In addition, those solutions associated with linear trends having strikes within 9° of east-west were discarded due to residual errors in flight-line processing that could not be removed. The remaining solutions were then interpolated as grids and contoured to represent minimum (Fig. 4a) and maximum (Fig. 4b) estimates of depth. The two plots use very different contour intervals to accommodate the large separations between depth solutions expected for increasing depth while still allowing comparison of patterns.

To first order, the contour plots of minimum and maximum estimates of depth have similar patterns. Both indicate depths are shallow on the west-central side of the survey area and deep close to the range front and in the mountains on the eastern side (compare

TABLE 1. Depths and thickness of basalt intervals found in water wells.

WELL NAME[1]	TOTAL DEPTH (METERS)	DEPTHS OF BASALT INTERVAL(S)[2] (METERS)	THICKNESS OF BASALT INTERVAL(S) (METERS)
Acequia WT	245	no basalt	0
BOR-2/BOR-3	617	176-?	?
BOR-4	541	228-289, 320-329	61, 9
BOR-5	551	521-551 TD	>30
Buffalo Pasture	213	no basalt	0
Don's Field	192	no basalt	0
K2	621	88-105, 128-143, 189-229	16, 15, 40
RP-2000	770	5-29, 49-143, 189-229	24, 18, 34
RWP-1	139	1-139 TD	>139
RWP-3	215	99-215 TD	>116
RWP-6	72	no basalt	-
Town Airport	524	11-18, 27-46, 55-146, 152-174	8, 18, 91, 21
Town Yard	311	120-146, 177-198	26, 21
Tract A PW#2	305	33-47, 63-86, 114-144, 150-156	14, 23, 30, 5
Tract B PW	954	180-259	79

[1]Wells are selected from those located on Plate 5a. Information is from records at the New Mexico Office of State Engineer, William White and Chris Banet of the Bureau of Indian Affairs, and Paul Drakos of Glorieta Geoscience, Inc.
[2]Well completed above the bottom of the basalt interval is noted by TD. Missing information is indicated where queried.

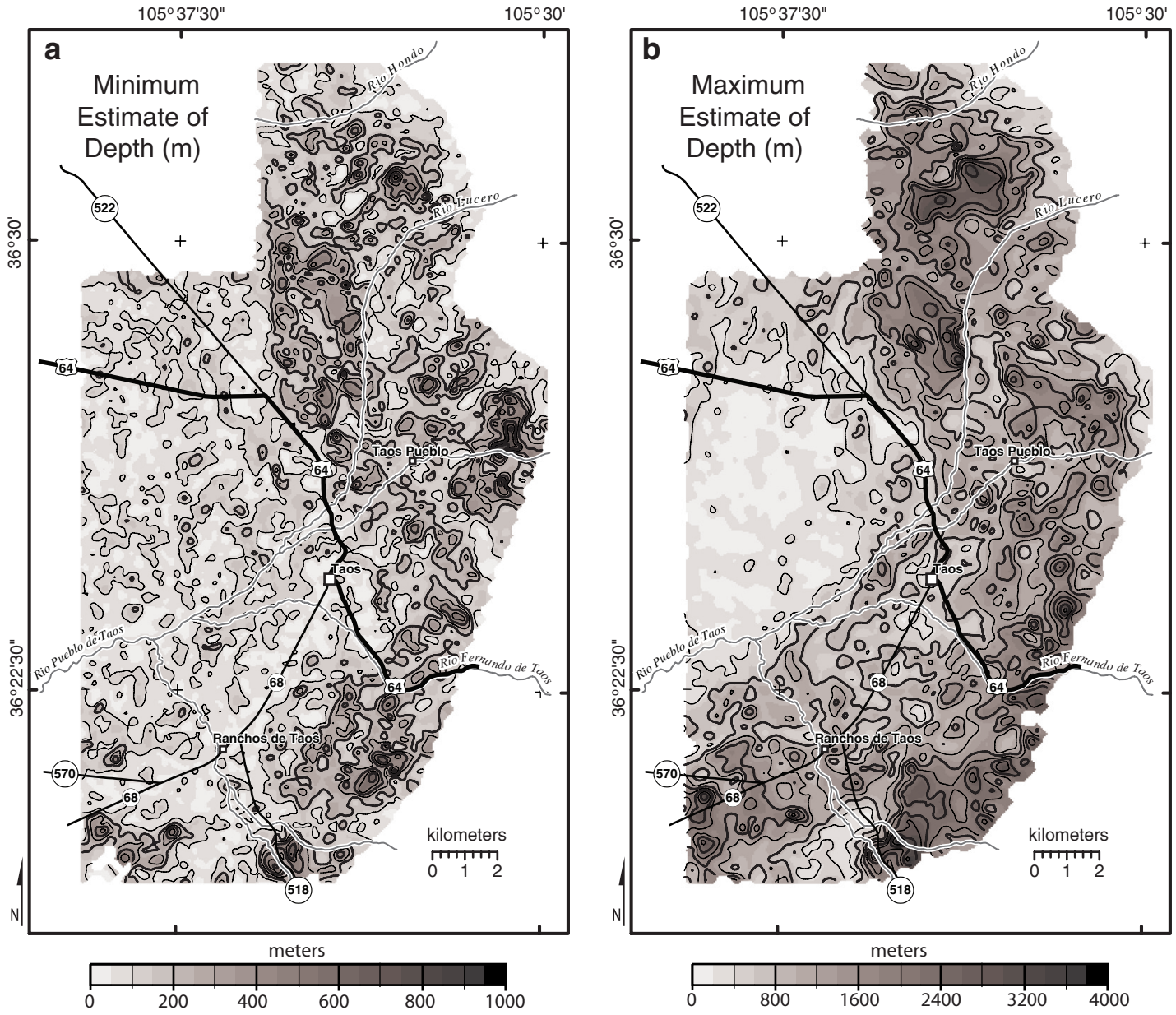

FIGURE 4. Contour maps of minimum and maximum estimates of depth to top of magnetic source from horizontal gradient analysis (Phillips, 2000; Phillips, 1997; program HDEP). Minimum estimates from HGM of RTP data (a). Maximum estimates from HGM of pseudogravity (b). These plots are intended to reveal overall depth patterns only; they are not reliable for predicting depth at specific locations (see text). Note that the range and contour intervals for the depth estimates from the HGM of the reduced-to-pole data are much smaller than for those from the HGM of the pseudogravity, which is expected from the larger separation between minimum and maximum estimates as the sources get deeper.

Figs. 1 and 4). Both show generally contrasting patterns that are bounded by Rio Hondo and Rio Lucero in the northeast, approximately 105°35'W longitude in the north center, about 1 km northeast of and parallel to US-64 heading southeast from Taos, and near NM-518 within the foothills southeast of Ranchos de Taos.

Systematic differences between the depth-estimate plots occur in the area of shallowest estimates in the northwestern structural domain (Figs. 3 and 4). The minimum estimates range from 0-200 m throughout the domain, whereas the maximum estimates increase from shallow (<800 m) to a larger range (0-1600 m) around the edges of the domain. This increase in vertical separation of the minimum and maximum estimates may indicate a systematic drop in depths to magnetic sources, analogous to the hypothetical model over the top edges of layers C and D (Fig. 2).

The areas of deepest estimates in both plots are similar, along the southern, eastern, and northeastern parts of the survey area (Fig. 4). In detail, both minimum and maximum estimates range widely, from 200-1000 m for the range of minima to 1000-4000 m for the range of maxima. In addition, the separation between minimum and maximum estimates does not vary consistently. The wide variability may be explained by multiple sources at different levels. This situation could be produced by anthropogenic sources, geologic variability, or noise in the data.

GEOLOGIC INTERPRETATION

In this section, we integrate quantitative analyses with qualitative analysis to arrive at a geologic interpretation. To facilitate discussion, we use the structural domains recognized from the patterns of magnetic source edges (Fig. 3 and Plate 5b) as general divisions. Within these, we have outlined and labeled smaller areas of interpreted features on Figure 5. The outlines are based on differences in magnetic patterns or inferred magnetic source, discussed in the qualitative analysis, and ranges of estimated depths determined from quantitative analysis (Fig. 4). Because the depth estimates give such large ranges, they are used only as approximate indicators of depth variations. Although the geologic outlines were drawn along inferred faults where possible, they do not always coincide with the structural domain boundaries, which rely on contrasts in fault patterns.

Northwestern Domain

The highly variable, high-amplitude (50-100 nT) negative anomalies in the west-central portion of the northwestern structural domain (<-550 nT; deep blue colors on Plate 5a) correspond to shallow, reversed-polarity Servilleta Basalt (near-surface R basalt on Fig. 5). Mapped geology (Plate 6), wells within or nearby the area (RP-2000, RWP-1, Tract A PW#2 on Table 1 and Plate 5a), and shallow depth estimates (Fig. 4) indicate the basalt is at or near the surface. The high-amplitude negative anomalies indicate that the basalt has dominant, reversed-polarity remanent magnetization. Because of the sensitivity of aeromagnetic data to the shallowest sources, the reversed-polarity basalt likely has significant thickness near the top of the basalt section.

Several north-trending positive linear anomalies cut the negative anomalies (Plate 5a) and correspond to interpreted magnetic source edges (Plate 5b). Such positive anomalies are expected over faults that offset magnetic units with dominant reversed-polarity magnetization (reversed-polarity basalt), as demonstrated by the basalt layers in the hypothetical model (Fig. 2). The interpreted magnetic source edges are likely related to the Los Cordovas faults (Fig 1; Kelson and Bauer, 2003), based on similar orientation and spacing. Moreover, two Los Cordovas fault exposures within the survey area north of the Rio Pueblo de Taos closely parallel or coincide with the inferred faults (Fig. 3).

Although the dominant throw of mapped Los Cordovas faults is west-down (Machette and Personius, 1984; Bauer and Kelson, 2004), depth estimates and anomaly patterns indicate that two east-down faults offset Servilleta Basalt on the east. One is a north-striking fault just east of 105°37'30"W longitude (Figs. 3 and 5), which coincides with a marked decrease in the amplitudes of negative anomalies (Plate 5a). The second is also north-striking, but farther east, near longitude 105°35"W, which marks the boundary between the northwestern and northeastern structural domains (Fig. 3). Depth-estimates show an abrupt contrast across this inferred fault, which is best displayed by more than 200 m difference in the minimum estimates along a sharp line (Fig. 4a). On the eastern side of this fault, in the northeastern structural domain, the basalt is too deep (521 m in BOR-5, Plate 5a) to likely have much affect on the magnetic field; the depth estimates are probably reflecting depths to crystalline basement. This easternmost interpreted east-down fault likely coincides with the west side of a graben interpreted from geologic and other geophysical evidence (Bauer and Kelson, 2001; Plate 7).

The pattern of high-amplitude negative anomalies abruptly changes just to the north of US-64 (Plate 5a). Both amplitudes and steepness of anomaly slopes are reduced. Depth estimates gradually increase to the north, which is most apparent in the plot of maximum estimates (Fig. 4b). Increased depths compared to the area to the south are corroborated by depths to basalt of about 100 m or greater in wells BOR-4, RWP-3, and Tract B PW (Plate 5a; Table 1). The increased depth is primarily due to a gradual rise in topography. For example, the difference in elevations at wells Tract B PW (2228 m or 7310 ft) and Tract A PW#2 (2067 m or 6780 ft) is 161 m, whereas the difference in elevation to the top basalt layers in the wells is only 14 m (Table 1). However, the gradual increase in topography does not explain the sharpness of the contrast between the different anomaly patterns. The contrast may be explained by a much thicker section of normal-polarity basalt overlying reversed-polarity basalt on the north (N/R basalt at different depths on Fig. 5). Flows with normal-polarity overlying those with reversed-polarity are consistent with the sequence of Servilleta basalt flows examined in the gorge (Brown et al., 1993). Variations in section to the north could have resulted from faulting followed by erosion. However, differences in the magnetic properties of the basalt could be also be caused by variations in thickness and physical properties that attended the original emplacement of the flows.

Southeastern and Southwestern Domains

The north-south fault patterns of the northwestern structural domain appear truncated by northeasterly faults within the southeastern structural domain, near Rio Pueblo de Taos (Figs. 3 and 5). Northeast-striking inferred faults parallel the Embudo fault zone in the vicinity of Ranchos de Taos then turn more northerly to parallel the Sangre de Cristo fault zone northeast of Taos (Fig. 3). The parallel faults persist within a zone near the range front that widens to the southwest from 2 km to 7 km. More northerly orientations of several inferred faults in the small, southwestern structural domain (Fig. 3), may reflect the influence of the north-striking Picuris-Pecos fault system (Fig. 1) where it underlies the basin (Bauer and Kelson, 2004).

The northeast-trending truncation at the southern edge of the northwestern structural domain roughly coincides with the Rio Pueblo de Taos (Fig. 5). Southeast of this truncation, negative anomalies (<-530 nT; medium to deep blue colors on Plate 5a) appear to extend in a northeast-trending swath throughout most of the central part of the survey area (mod. depth and deep R basalt on Fig. 5). Subdued anomaly amplitudes and increased maximum estimates of depth suggest the basalt is somewhat deeper here compared to the areas of shallow basalt. Previous workers have suggested that the Rio Pueblo de Taos coincides with the axis of a small-amplitude syncline (e.g., Machette and Personius, 1984). The aeromagnetic patterns, depth estimates, and locations of

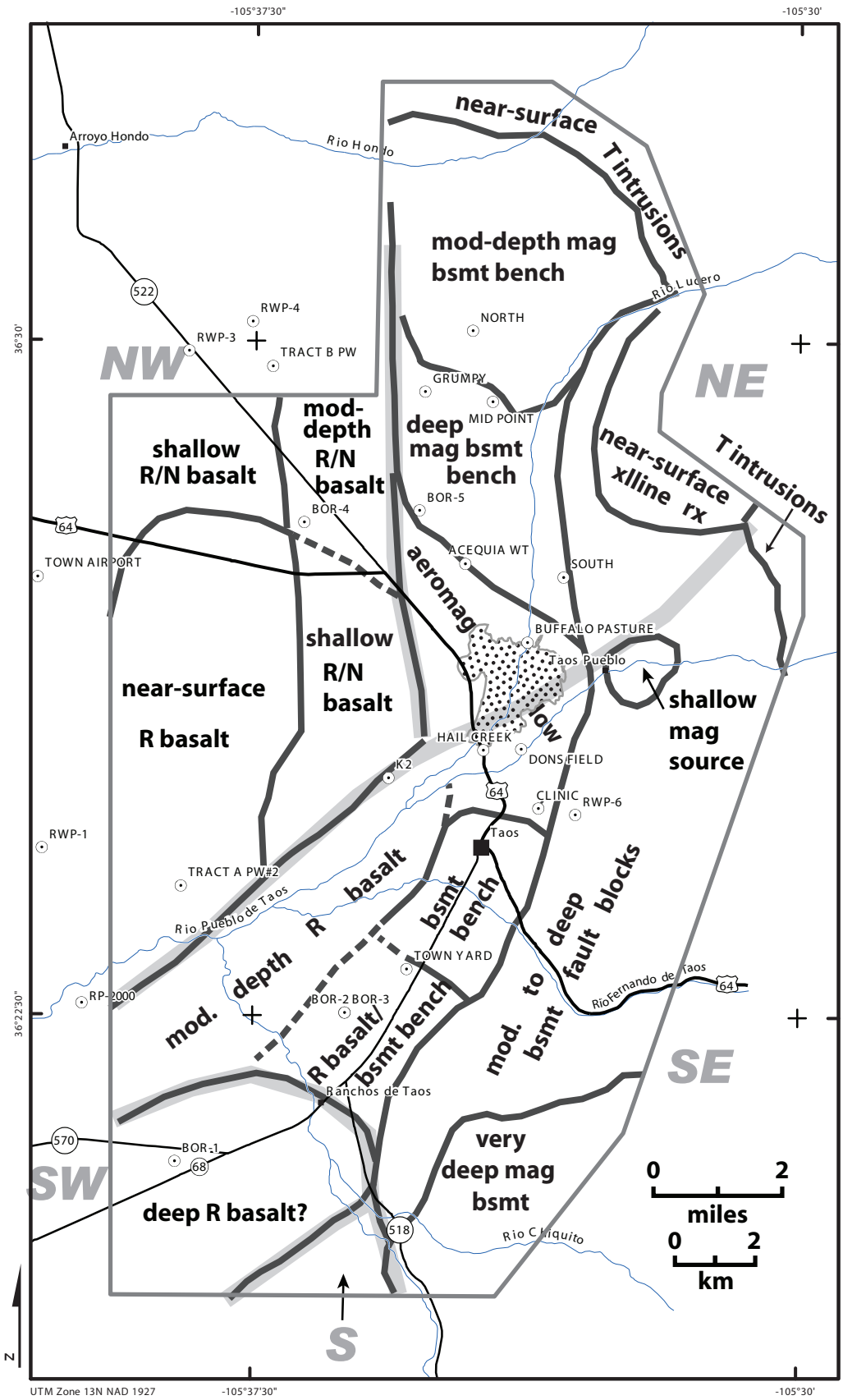

TERMINOLOGY FOR INTERPRETATIONS

R basalt
Basalt with dominant reversed-polarity remanent magnetization (reversed-polarity basalt)

N/R basalt
Normal-polarity basalt overlying reversed-polarity basalt

bsmt
Precambrian crystalline basement rocks

mag
Magnetic; having moderately high total magnetization

aeromag low
Area of low aeromagnetic values

T intrusions
Tertiary intrusive rocks

xlline rx
Precambrian crystalline rocks

SYMBOLS

Buffalo Pasture marshlands

Outline of interpretive area described in text

Structural domain boundary and label

RWP-4 Well location

Figure 5 - Geologic interpretations discussed in text. Area is divided into the general structural domains of Figure 3, and subdivided into interpretive areas based on differences in anomaly pattern, inferred magnetic source, and depth estimates.

magnetic source edges suggest a fault system that generally follows the river valley and truncates the southern extent of the Los Cordovas faults in a southeast-down sense. The fault system may be associated with a syncline. Truncation of the Los Cordovas faults is also indicated by lack of any geologic evidence for their extension south of the river (Bauer and Kelson, 1997; Kelson and Bauer, 2003).

The low aeromagnetic values near the Rio Pueblo de Taos do not extend far inside the limits of the Town of Taos (white outline on Plate 5a), where aeromagnetic values are somewhat higher (-470 to -500 nT; bsmt bench on Fig. 5). Shallow basement is indicated by eroded Pennsylvanian limestone encountered at about 300 m depth in the nearby Town Yard well (Bauer and Kelson, 2004; Plate 5a). The well, which encountered basalt at moderate levels (120 m, Table 1), is located where aeromagnetic values are locally somewhat lower (approximately -530 nT). Another local low near Rio Fernando de Taos (FL on Plate 5a), on the edge of the town limits, is bounded by an inferred mapped fault and crosses a residential neighborhood with no apparent influence from the effects of anthropogenic structures. The limited lateral extent of the low allows us to speculate that reversed-polarity basalt may be very locally preserved over a basement high in this area. If true, then basalt is mostly absent throughout the rest of the Town area, but covers the structural bench to the south (R basalt/bsmt bench on Fig. 5). On the other hand, non-geologic sources that cluster to produce overall higher aeromagnetic values in the Town area may mask reversed-polarity basalt.

The basement bench under Taos likely extends southwest and northeast of Taos, bounded on the west by the Town Yard fault (Bauer and Kelson, 2004). We have drawn an equivalent fault to coincide with a north-northeast-striking inferred fault (Fig. 3) that generally marks a contrast in anomaly character (west side of bsmt bench near Taos on Fig. 5; Plate 5a) and speculate that it continues southeast past Ranchos de Taos (R basalt/bsmt bench on Fig. 5).

The extension of the Town Yard fault and the basement bench are unclear to the north where a large area of low aeromagnetic values corresponds to the marshlands of Buffalo Pasture (aeromag low on Fig. 5; Plate 5a). This low straddles the boundary between the northeastern and southeastern structural domains (Fig. 5), indicating structural complexity. This complexity, interference from anthropogenic sources along US-64, and lack of surface exposures combine to make interpretation of basement structural blocks in this area ambiguous. Moderately deep estimates to the top of magnetic sources (200-400 m minimum and 800-1000 m maximum on Fig. 4) and the negative aeromagnetic values suggest the presence of reversed-polarity basalt at depth. Alternatively, the negative values reflect an overall decrease in magnetization of the Precambrian basement compared to that under the Town of Taos. Detection of moderately deep magnetic sources in the area may reflect local lithologic variations in the Precambrian basement rocks.

A shallow magnetic source (100-500 m deep estimated from Fig. 4) is interpreted at the northern end of the southeastern domain, straddling Rio Pueblo de Taos just east of Taos Pueblo (shallow mag source on Fig. 5). The area of the positive anomaly coincides with a graben interpreted from shallow seismic-reflection and gravity data (Reynolds, 1986, 1992). The magnetic source may be detritus from the magnetic crystalline rocks to the north that filled the graben during Tertiary time, perhaps analogous or synchronous with the Picuris Formation, exposed in the vicinity of the Picuris-Pecos fault (Bauer et al., 1999b; Bauer and Kelson, 2004).

In the mountains on the eastern part of the southeastern structural domain, aeromagnetic anomalies corresponding to exposures of Paleozoic sedimentary rocks range in value from -500 to -420 nT (green, yellow, and orange colors on Plate 5a). Because the magnetic properties of the Paleozoic rocks are expected to be low, these anomalies are probably due to underlying Precambrian basement (mod. to deep bsmt fault blocks on Fig. 5). The low amplitudes of the anomalies suggest the Precambrian rocks are weakly to moderately magnetic, consistent with their lack of expression in regional aeromagnetic maps (Plate 4; Grauch and Keller, 2004). The variable anomaly pattern and wide-ranging, inconsistent depth estimates (Fig. 4 and very deep mag bsmt on Fig. 5) may reflect the high variability in lithology and magnetic properties expected of Precambrian rocks rather than structural relief. The most magnetic part of the basement is represented by a positive ~30-nT-amplitude anomaly at the southeastern limits of the Town of Taos (SEL on Plate 5a). The anomaly has a curvilinear western edge that is parallel to, but about 400 m to the northwest of, mapped faults (Plate 5a). This edge gives depth estimates that range from 400-1000 m (Fig. 4). The shift in location from the mapped faults may be a product of viewing the fault plane downdip from the surface exposures, where the Precambrian basement underlies 400-1000 m of effectively nonmagnetic material (probably Paleozoic section).

Northeastern Domain

The northeastern structural domain is characterized by inferred faults that are crossing, irregularly spaced, and oriented north, northeast, and northwest (Fig. 3). The largest, and broadest magnetic gradients follow the northwest-striking inferred faults. In contrast, the north- and northeast-striking inferred faults are associated with more local gradients (Plate 5a). The northwest strikes of the inferred faults may indicate a pre-Tertiary origin, based on the relations between inferred and mapped faults at the easternmost point of the survey area. Here, an inferred fault generally coincides with the major, Paleozoic or older fault that juxtaposes Precambrian against Paleozoic rocks northwest of Taos Pueblo (Baltz and Myers, 1999; Plate 6; Fig. 3). The north-striking faults may be rift-related, because of their orientation. Several of them align with Rio Lucero (Fig. 3), which indicates a tectonic control on the development of the drainage.

Extremely high values (-420 to 100 nT) occur along the northern perimeter of the survey area, north of where the survey boundary intersects Rio Lucero (Plate 5a). Similar high values occur in the far eastern corner of the survey area, corresponding to mapped Paleozoic sedimentary rocks (PH on Plate 5a). Despite the appearance of the color display, anomalies along the survey boundary between these two areas have lower values (-

400 to -350 nT). The northernmost area of high values is part of a regional-scale, northwest trending alignment of positive aeromagnetic anomalies (Saladan Creek fault on Plate 4). The regional aeromagnetic trend is best explained by magnetic igneous rocks that were emplaced along a pre-existing fault during Tertiary time (Grauch and Keller, 2004). This conclusion, and the lack of strong expression of Precambrian rocks in the regional aeromagnetic data to the north of the survey area (Grauch and Keller, 2004), suggests that Tertiary intrusions are the primary source of the high-amplitude aeromagnetic anomalies in the northern part of the survey area (near-surface T intrusions on Fig. 5).

Positive anomalies with similar amplitudes extend southwestward from the northwest alignment on the regional map (Plate 4) and reach into the far eastern part of the high-resolution survey area (PH on Plate 5a). These high values may be caused by Tertiary intrusive rocks (easternmost T intrusions on Fig. 5), which are related to those along the northwest alignment and underlie the Paleozoic sedimentary rocks mapped in the area (Plate 5a). This scenario fits with the lack of geologic evidence for major structural offset across the Rio Pueblo de Taos (Bauer and Kelson, 2001). In contrast, the area of lower aeromagnetic values, south of Rio Lucero, may be caused by moderately magnetic Precambrian basement (near-surface xlline rx on Fig. 5). Magnetic susceptibility measurements of the exposed Tertiary and Precambrian rocks in the area would help evaluate these interpretations.

Away from the magnetic rocks in the mountains, the aeromagnetic patterns and depth estimates suggest that crystalline basement rocks are at successively lower structural levels to the south and west. The blocks are bounded primarily by the northwest- and north-trending inferred faults. The deepest interpreted basement block (deep mag bsmt bench) is associated with minimum and maximum depth estimates that are both large (200-400 m and 1600-2400 m on Fig. 4). It must be noted that depths to the structural blocks in the survey area represent depths to the magnetic crystalline basement, not to the overlying Paleozoic rocks, which may vary in thickness over the crystalline basement.

Southern Domain

In the southern domain, positive and negative anomalies (30-50 nT amplitude) are located at the structurally complex intersection of the Picuris-Pecos, Embudo, and Sangre de Cristo fault systems (Fig. 1 and Plate 5a). Positive anomalies follow a semi-circular pattern around an elongate northwest-trending positive anomaly, flanked by negative anomalies. The elongate positive anomaly corresponds to topographically high exposures of Precambrian granite (Miranda granite of Kelson and Bauer, 2003). The negative anomalies that flank this elongate anomaly likely arise from the sharp contact between the granite and effectively nonmagnetic rock units, such as the Paleozoic sedimentary rocks that lie on the northwest flank (Plate 6). The small positive anomalies in the semi-circular pattern generally follow local outcrops of Tertiary Picuris Formation. This formation consists of conglomeratic sandstone that commonly contains volcanic clasts and includes a ridge-forming unit of volcanic breccia (Bauer et al., 1999b; Bauer and Kelson, 2004). The small positive anomaly that spans Rio Chiquito and NM-518 (Plate 5a) near their intersection does not have a corresponding outcrop, but may indicate that Picuris Formation is buried in this location. If so, the anomaly supports geologic mapping suggesting that strands of the Embudo fault zone can be extended eastward along the northern side of the anomaly (Plates 5a and 6).

SUMMARY

High-resolution aeromagnetic data were recently collected in an area surrounding the Town of Taos. Preliminary qualitative and quantitative analyses of the data were integrated to gain a first look at information provided on subsurface geology. The primary magnetic sources expressed in the aeromagnetic data are interpreted as Servilleta Basalt, Precambrian crystalline basement, and Tertiary intrusions. The Tertiary volcaniclastic Picuris Formation may also locally produce positive anomalies. Servilleta Basalt is typically associated with negative anomalies, indicating a dominant, reversed-polarity remanent magnetization (reversed-polarity basalt). However, in the northwestern portion of the survey area, we suspect that the Servilleta Basalt section is composed of normal-polarity flows overly reversed-polarity flows.

The western part of the survey area is dominated by strong negative anomalies and prominent north-trending linear gradients that we attribute to shallow Servilleta Basalt cut by faults related to the Los Cordovas faults, which are exposed to the west. The basalt is successively faulted down to the east until it is no longer detectable in the aeromagnetic data above the magnetic basement. On the south, the basalt and related north-south faulting are truncated and faulted down to the southeast along northeast-trending, inferred faults that generally follow the Rio Pueblo de Taos. The northeast fault orientation parallels the Embudo fault zone in the south, becoming more northerly to the northeast, where the inferred faults parallel and follow the range-bounding Sangre de Cristo fault zone east of Taos. The parallel faults, which span a 2- to 7-km-wide zone westward of the range front faults, suggest a persistent influence of this faulting into the basin. A few north-striking faults southwest of Ranchos de Taos may reflect the influence of the Picuris-Pecos fault system, where it underlies the basin.

Some of the inferred northeast-striking faults appear to bound the western side of a previously known (Bauer and Kelson, 2004) basement structural bench under the Town of Taos. From the contrasting negative and positive anomaly patterns, we speculate that the bench is irregularly overlain by Servilleta Basalt. The configuration of the basement bench is difficult to follow to the north, where it appears to extend into a large magnetic low centered over Buffalo Pasture marshland. Buffalo Pasture is located in a structurally complex area, evidenced by the convergence of inferred faults of several different orientations. More work is required to understand the aeromagnetic low in this area.

We interpret the data in the northeastern portion of the survey area to primarily represent several structural blocks that drop basement generally southwestward along north- and northwest-striking faults. The north-striking inferred faults generally follow and parallel Rio Lucero, indicating that this river, like Rio Pueblo

de Taos, is tectonically controlled. The area also includes magnetic rocks in the mountains that we attribute to Tertiary intrusions, most of which are exposed north of the survey area. Just north of Rio Pueblo de Taos, we propose that a Tertiary intrusion lies beneath Paleozoic sedimentary rocks.

Much more could be learned from the aeromagnetic data through detailed examination of data along flight lines and incorporation of much more geologic, drillhole, and geophysical information. In the meantime, the data have improved our regional view of the geologic framework of the subsurface and have pointed out several places where ambiguities need to be resolved.

ACKNOWLEDGMENTS

Funding for acquisition or interpretation of the high-resolution aeromagnetic data was provided by the Town of Taos, Taos Soil and Water Conservation District, Taos County, Bureau of Indian Affairs, Bureau of Reclamation, and the New Mexico Office of the State Engineer. We are grateful to Adam Read for his invaluable assistance with the illustrations. Reviews by Scott Baldridge, Viki Bankey, and Jeff Phillips resulted in valuable improvements to the paper.

REFERENCES

Appelt, R.M., 1998, $^{40}Ar/^{39}Ar$ geochronology and volcanic evolution of the Taos Plateau volcanic field, northern New Mexico and southern Colorado [MS thesis], New Mexico Institute of Mining and Technology, Socorro, NM.

Baltz, E.H., and Myers, D.A., 1999, Stratigraphic framework of upper Paleozoic rocks, southeastern Sangre de Cristo Mountains, New Mexico, with a section on speculations and implications for regional interpretation of Ancestral Rocky Mountain paleotectonics: New Mexico Bureau of Mines and Mineral Resources Memoir 48, 269 p.

Bankey, V., Grauch, V.J.S., and Fugro Airborne Surveys Corp., 2004, Digital aeromagnetic data and derivative products from a helicopter survey over the Town of Taos and surrounding areas, Taos County, New Mexico: U. S. Geological Survey Open-file report 2004-1229a, CD-ROM.

Baranov, V., 1957, A new method for interpretation of aeromagnetic maps: pseudo-gravimetric anomalies: Geophysics, v. 22, p. 359-383.

Bauer, P.W., 1993, Proterozoic tectonic evolution of the Picuris Mountains, northern New Mexico: Journal of Geology, v. 101, p. 483-500.

Bauer, P.W., Johnson, P.S., and Kelson, K.I., 1999a, Geology and hydrogeology of the southern Taos Valley, Taos County, New Mexico: Final Technical Report for the New Mexico Office of the State Engineer, January 1999, 56 p.

Bauer, P.W., and Kelson, K.I., 1997, Geology of the Taos SW 7.5' quadrangle, Taos County, New Mexico: New Mexico Bureau of Mines and Mineral Resources Open-file Geologic Map OF-GM 43, scale 1:12,000.

Bauer, P.W., and Kelson, K.I., 2001, Geology of the Taos 7.5-minute quadrangle, Taos County, New Mexico: New Mexico Bureau of Mines and Mineral Resources Open-file Geologic map OF-GM 43, scale 1:12,000.

Bauer, P.W., and Kelson, K.I., 2004, Cenozoic structural development of the Taos area, New Mexico: New Mexico Geological Society, 55th Field Conference, Guidebook, p. 129-146.

Bauer, P.W., Kelson, K.I., Lyman, J., Heynekamp, M.R., and McCraw, D.J., 1999b, Geology of the Ranchos de Taos 7.5-minute quadrangle, Taos County, New Mexico: New Mexico Bureau of Mines and Mineral Resources Open-file Geologic Map OF-GM 33, scale 1:12,000.

Bauer, P.W., and Ralser, S., 1995, The Picuris-Pecos fault--repeatedly reactivated, from Proterozoic(?) to Neogene: New Mexico Geological Society, 46th Field Conference, Guidebook, p. 111-115.

Blakely, R.J., 1995, Potential theory in gravity and magnetic applications: Cambridge University Press, 441 p.

Blakely, R.J., and Simpson, R.W., 1986, Approximating edges of source bodies from magnetic or gravity anomalies: Geophysics, v. 51, p. 1494-1498.

Brown, L.L., Caffall, N.M., and Golombek, M.P., 1993, Paleomagnetism and tectonic interpretations of the Taos Plateau volcanic field, Rio Grande rift, New Mexico: Journal of Geophysical Research, v. 98, p. 22,401-22,413.

Butler, R.F., 1992, Paleomagnetism: Magnetic domains to geologic terranes: Boston, Blackwell Scientific, 319 p.

Clark, D.A., 1997, Magnetic petrophysics and magnetic petrology; aids to geological interpretation of magnetic surveys: AGSO Journal of Australian Geology and Geophysics, v. 17, p. 83-103.

Cordell, L., and Grauch, V.J.S., 1985, Mapping basement magnetization zones from aeromagnetic data in the San Juan Basin, New Mexico, *in* Hinze, W.J., ed., The Utility of Regional Gravity and Magnetic Anomaly Maps: Society of Exploration Geophysicists: Tulsa, Oklahoma, p. 181-197.

Cordell, L., and Keller, G.R., 1984, Regional structural trends inferred from gravity and aeromagnetic data in the New Mexico-Colorado border region: New Mexico Geological Society, 35th Field Conference, Guidebook, p. 21-23.

Drakos, P., and Lazarus, J., 1998, Hydrogeologic characterization, surface water-ground water interaction, and water quality in the southern San Luis Basin in the vicinity of Taos, NM, Proceedings of the 1998 Ground water Protection Council Annual Forum, p. 104-114.

Dungan, M.A., Muehlberger, W.R., Leininger, L., Peterson, C., McMillan, N.J., Gunn, G., Lindstrom, M., and Haskin, L., 1984, Volcanic and sedimentary stratigraphy of the Rio Grande gorge and the Late Cenozoic geologic evolution of the southern San Luis valley: New Mexico Geological Society, 35th Field Conference, Guidebook, p. 157-170.

Faulds, J.E., and Varga, R.J., 1998, The role of accommodation zones and transfer zones in the regional segmentation of extended terranes, *in* Faulds, J.E., and Stewart, J.H., eds., Accommodation Zones and Transfer Zones: The Regional Segmentation of the Basin and Range Province: Boulder, CO, Geological Society of America Special Paper 323, p. 1-45.

Grauch, V.J.S., 1999, Principal features of high-resolution aeromagnetic data collected near Albuquerque, New Mexico: New Mexico Geological Society, 50th Field Conference, Guidebook, p. 115-118.

Grauch, V.J.S., and Bankey, V., 2003, Aeromagnetic interpretations for understanding the hydrogeologic framework of the southern Española Basin, New Mexico: U. S. Geological Survey Open-file Report 03-124

Grauch, V.J.S., Hudson, M.R., and Minor, S.A., 2001, Aeromagnetic expression of faults that offset basin fill, Albuquerque basin, New Mexico: Geophysics, v. 66, p. 707-720.

Grauch, V.J.S., and Keller, G.R., 2004, Gravity and aeromagnetic expression of tectonic and volcanic elements of the southern San Luis Basin, New Mexico and Colorado: New Mexico Geological Society, 55th Field Conferecne, Guidebook, p. 230-243.

Grauch, V.J.S., Rodriguez, B.D., and Deszcz-Pan, M., 2002, How geophysical methods have been used to understand the subsurface, *in* Bartolino, J.R., and Cole, J.C., eds., Ground-water resources of the Middle Rio Grande Basin, New Mexico, U.S. Geological Survey Circular 1222, p. 36-37.

Hudson, M.R., Mikolas, M., Geissman, J.W., and Allen, B., 1999, Paleomagnetic and rock magnetic properties of Santa Fe group sediments in the 98th Street core hole and correlative surface exposures, Albuquerque Basin, New Mexico: New Mexico Geological Society, 50th Field Conference, Guidebook, p. 355-362.

Hudson, M.R., Thompson, R.A., Barbá, K.E., Grauch, V.J.S., Sawyer, D.A., and Warren, R.G., 2004, Paleomagnetism as a link between geologic and aeromagnetic mapping of the Cerros del Rio volcanic field, Rio Grande rift, New Mexico, *in* Hudson, M.R., ed., Geologic and Hydrogeologic Framework of the Española Basin -- Proceedings of the 3rd Annual Española Basin Workshop, Santa Fe, New Mexico, March 2-3, 2004: U. S. Geological Survey Open-file Report 2004-1093, p. 31.

Keller, G.R., Cordell, L., Davis, G.H., Peeples, W.J., and White, G., 1984, A geophysical study of the San Luis Basin: New Mexico Geological Society, 35th Field Conference, Guidebook, p. 51-57.

Kelson, K.I., and Bauer, P.W., 2003, Geology of the Los Cordovas 7.5' quadrangle, Taos County, New Mexico: New Mexico Bureau of Geology and Mineral Resources Open-file Geologic Map OF-GM 63, scale 1:24,000.

Kelson, K.I., Bauer, P.W., Unruh, J.R., and Bott, J.D.J., 2004, Late Quaternary characteristics of the northern Embudo fault, Taos County, New Mexico: New Mexico Geological Society, 55th Field Conference, Guidebook, p.147-157.

Lambert, P.W., 1966, Notes of the late Cenozoic geology of the Taos-Questa area, New Mexico: New Mexico Geological Society, 17th Field Conference, Guidebook, p. 43-50.

Leininger, R.L., 1982, Cenozoic evolution of the southernmost Taos plateau, New Mexico [M.S. thesis]: Austin, TX, University of Texas, 110 p.

Lipman, P.W., and Reed, J.C., Jr., 1989, Geologic Map of the Latir Volcanic Field and Adjacent Areas, Northern New Mexico: U. S. Geological Survey 1:48000.

Machette, M.N., and Personius, S.F., 1984, Map of Quaternary and Pliocene faults in the eastern part of the Aztec 1° x 2° quadrangle and the western part of the Raton 1° x 2° quadrangle, northern New Mexico, U. S. Geological Survey Miscellaneous Field Studies Map MF-1465-A, scale 1:250,000.

Muszala, S., Stoffa, P.L., and Lawver, L.A., 2001, An application for removing cultural noise from aeromagnetic data: Geophysics, v. 66, p. 213-219.

New Mexico Bureau of Geology and Mineral Resources, 2003, Geologic Map of New Mexico, 1:500,000, New Mexico Bureau of Geology and Mineral Resources.

Phillips, J.D., 1997, Potential-field geophysical software for the PC, version 2.2: U.S. Geological Survey Open-File Report 97-725, p.

Phillips, J.D., 2000, Locating magnetic contacts: a comparison of the horizontal gradient, analytic signal, and local wavenumber methods: 70th Meeting, SEG, Calgary, Expanded Abstracts.

Phillips, J.D., and Grauch, V.J.S., 2004, Thickness of Santa Fe Group sediments in the Española Basin south of Santa Fe, New Mexico, as estimated from aeromagnetic data: U. S. Geological Survey Open-file Report, in press.

Reynolds, C.B., 1986, Shallow seismic reflection survey, Taos Pueblo, Taos County, New Mexico: Charles B. Reynolds and Associates Report to the BIA, May 27 10 p.

Reynolds, C.B., 1992, Shallow seismic reflection survey, northern Taos Pueblo area, Taos County, New Mexico: Charles B. Reynolds and Associates Report to the BIA, May 18 9 p.

Reynolds, R.L., Rosenbaum, J.G., Hudson, M.R., and Fishman, N.S., 1990, Rock magnetism, the distribution of magnetic minerals in the Earth's crust, and aeromagnetic anomalies: U. S. Geological Survey Bulletin 1924, 24-45 p.

PLATE 5: HIGH-RESOLUTION AEROMAGNETIC DATA – TAOS AREA

V.J.S. Grauch, Paul W. Bauer, and Keith I. Kelson

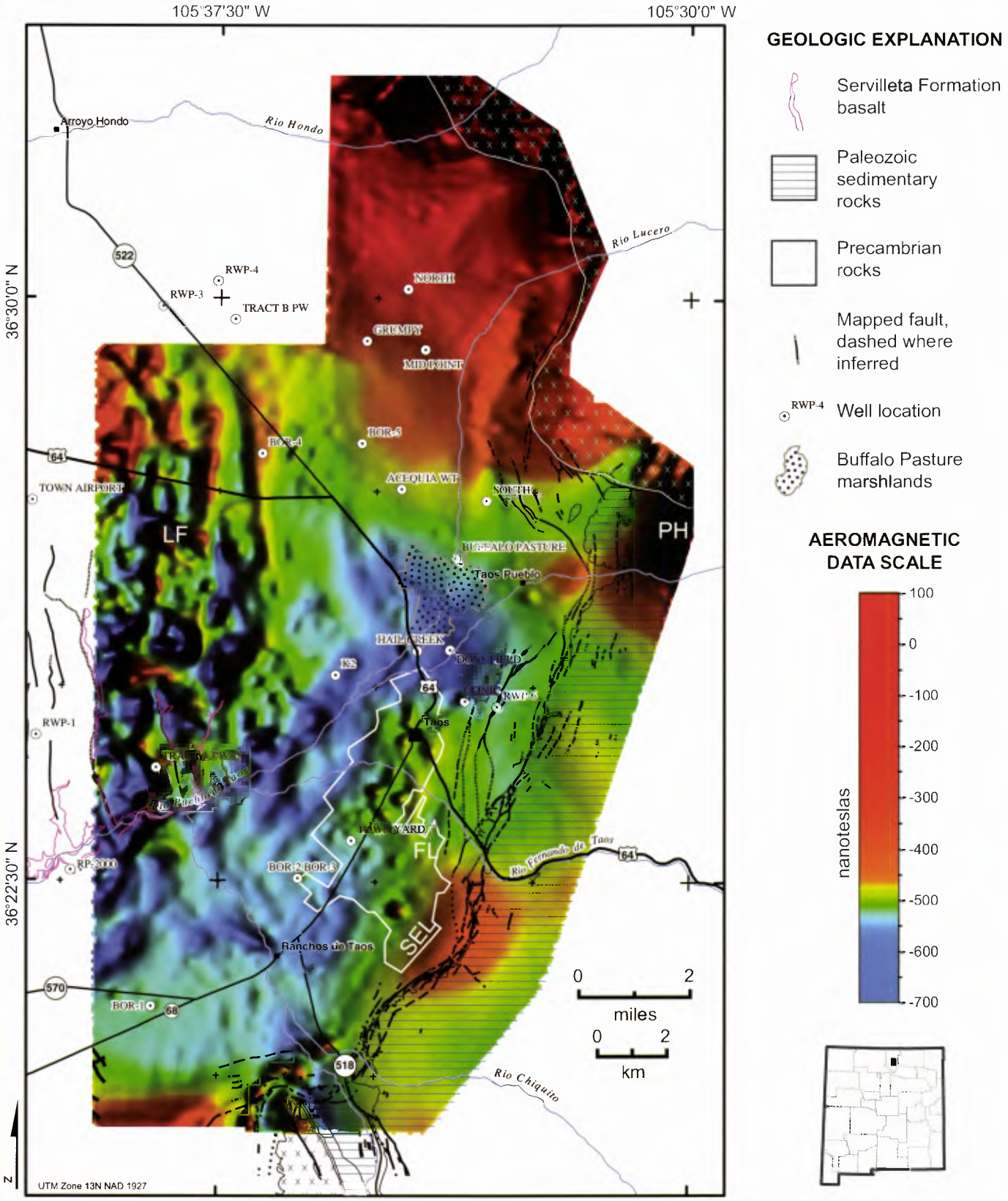

PLATE 5a. Color shaded relief image of reduced-to-pole (RTP), downward-continued, high-resolution aeromagnetic data for the Taos area. White outline indicates the limits of the Town of Taos. LF=landfill. FL=aeromagnetic low near Rio Fernando de Taos. SEL = aeromagnetic high just outside southeast town limits. See Grauch et al. (2004, this volume) for discussion.

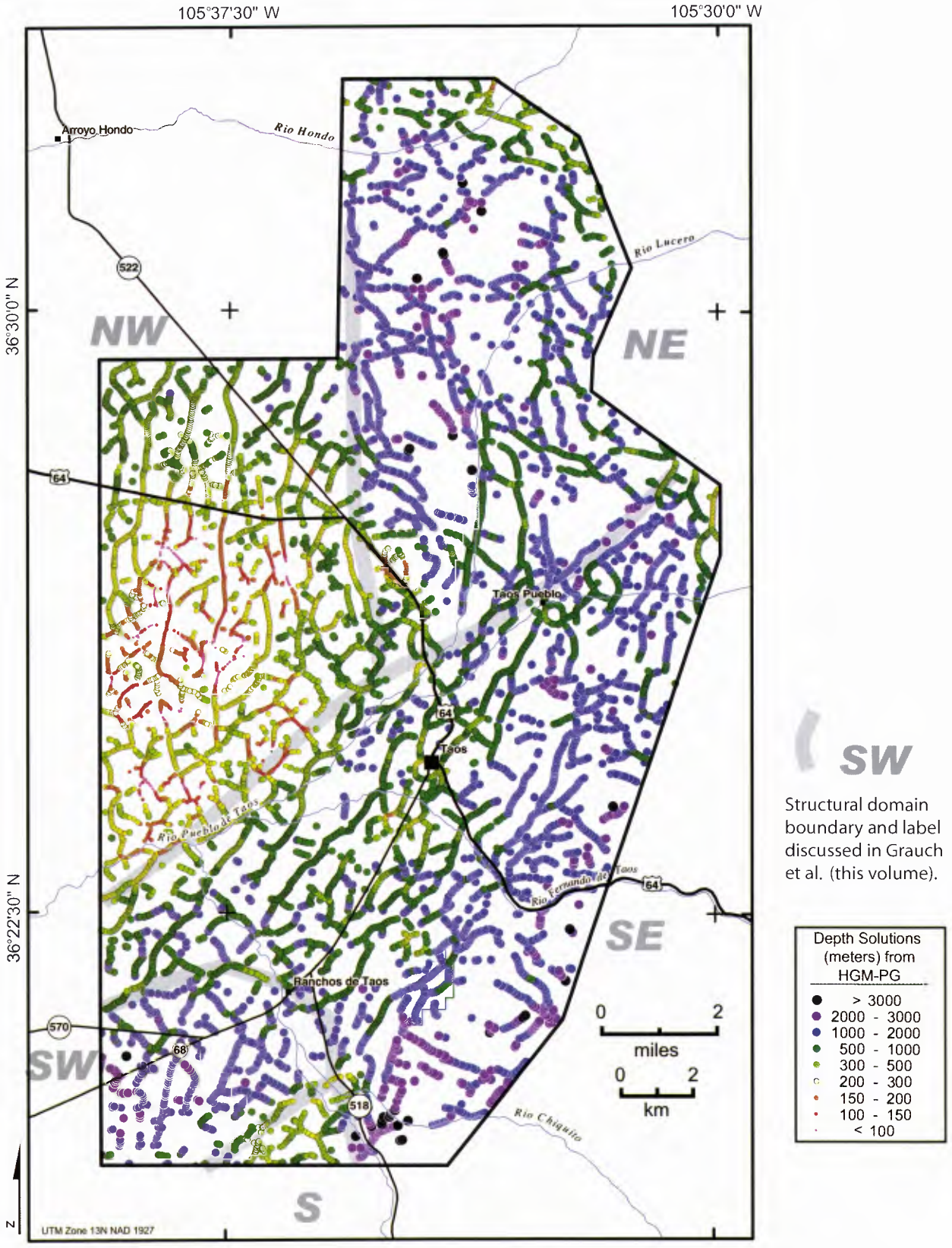

PLATE 5b. Maximum estimates of depth (meters) to the tops of magnetic source edges computed from the horizontal gradient magnitude of pseudogravity (HGM-PG), which is derived from aeromagnetic data (Plate 5a). Each point is an individual solution computed within a moving window across the grid. See Grauch et al. (2004, this volume) for discussion.